# UCLA
## UCLA Previously Published Works

**Title**

In utero electroporation-based translating ribosome affinity purification identifies age-dependent mRNA expression in cortical pyramidal neurons

**Permalink**

https://escholarship.org/uc/item/4wr658b8

**Authors**

Huang, Tianxiang
Nguyen, Lena H
Lin, Tiffany V
<u>et al.</u>

**Publication Date**

2019-06-01

**DOI**

10.1016/j.neures.2018.05.006

**Copyright Information**

Peer reviewed

# HHS Public Access

# In utero electroporation-based translating ribosome affinity purification identifies age-dependent mRNA expression in cortical pyramidal neurons

**Tianxiang Huang**[1,2], **Lena Nguyen**[2], **Tiffany V. Lin**[2], **Xuan Gong**[1,2], **Longbo Zhang**[1,2], **Gi Bum Kim**[3], **Matthew R. Sarkisian**[4], **Joshua Breunig**[3,5], and **Angelique Bordey**[1,2]

[1]Department of Neurosurgery, Xiangya Hospital, Central South University, 85 Xiangya Street, Changsha, 410008, China

[2]Departments of Neurosurgery, and Cellular & Molecular Physiology, Yale University School of Medicine, 333 Cedar Street, New Haven, CT 06520-8082, USA

[3]Board of Governors Regenerative Medicine Institute, Center for Neural Science and Medicine, and Department of Biomedical Science Cedars-Sinai Medical Center, Los Angeles, CA 90048

[4]Department of Neuroscience, McKnight Brain Institute, University of Florida, Gainesville, FL 32610

[5]Department of Medicine, David Geffen School of Medicine, UCLA, Los Angeles, CA, 90095, USA

## Abstract

We combined translating ribosome affinity purification (TRAP) with in utero electroporation (IUE), called iTRAP to identify the molecular profile of specific neuronal populations during neonatal development without the need for viral approaches and FACS sorting. We electroporated a plasmid encoding EGFP-tagged ribosomal protein L10a at embryonic day (E) 14–15 to target layer 2–4 cortical neurons of the somatosensory cortex. At three postnatal (P) ages—P0, P7, and P14—when morphogenesis occurs and synapses are forming, TRAP and molecular profiling was performed from electroporated regions. We found that ribosome bound (Ribo)-mRNAs from ~7,300 genes were significantly altered over time and included classical neuronal genes known to decrease (e.g., *Tbr1, Dcx*) or increase (e.g., *Eno2, Camk2a, Syn1*) as neurons mature. This approach led to the identification of specific developmental patterns for Ribo-mRNAs not previously reported to be developmentally regulated in neurons, providing rationale for future examination of their role in selective biological processes. These include upregulation of *Lynx1, Nrn1, Cntnap1* over time; downregulation of *St8sia2* and *Draxin*; and bidirectional changes to *Fkbp1b*. iTRAP is a versatile approach that allows researchers to easily assess the molecular profile

of specific neuronal populations in selective brain regions under various conditions, including overexpression and knockdown of target genes, and in disease settings.

## Keywords

TRAP; corticogenesis; migration; spine; glutamatergic neurons

## Introduction

Cortical neuron development follows well-established patterns of development from birth to synaptic integration that are governed by sequential gene expression. Gene profiling to identify the transcriptomic profile of selective cortical neuron populations has been described using a combination of antigenic neuron-specific labeling and fluorescence-activated cell sorting (FACS) from E15 to P1 (Molyneaux et al., 2007). Additional approaches have been developed to identify translating mRNA as an alternative to obtaining a proteomic profile of selective cell populations. This approach, called translating ribosome affinity purification (TRAP), has been used in combination with transgenic mice and viral approaches to assess the molecular profile of selective cell types (Cook-Snyder et al., 2015; Drane et al., 2014; Heiman et al., 2014; Heiman et al., 2008). Although all these approaches have been successful, they depend on mastering FACS for small neuronal populations, using transgenic mice or viral vectors. A recent study combined TRAP with in utero electroporation (IUE) to target layer 2/3 pyramidal neurons and perform qRT-PCR for 384 genes under condition of a specific gene knockdown compared to control (Rannals et al., 2016). They called the technique iTRAP. Here, we examined whether we could use iTRAP during cortical development and assess ribosome-bound (Ribo-) mRNA at different times after birth. In light of the inside-out development of the cerebral cortex and dilution of episomal plasmids, IUE at different embryonic ages allows expression of plasmids in selective populations of cortical pyramidal neurons located in a particular cortical region (Tabata and Nakajima, 2001). Neurons are generated from radial glia and migrate along the radial fiber to reach their specific layer by P7. Axogenesis occurs during and after migration while dendrite and spine development actively starts around P7 until P21, at which point pruning occurs (Kwan et al., 2012).

Here, we perform iTRAP at E14-E15 to target layer 2–4 pyramidal neurons and assess Ribo-mRNA in this population at three developmental hallmarks: P0, P7, and P14. We identified significant changes in Ribo-mRNA of ~7,300 genes over time. Gene ontology analysis confirmed that genes associated with biological processes such as ion transport, synaptic transmission and plasticity, dendrite extension, and G-protein coupled receptor signaling were enriched in Ribo-mRNAs that increased over time. Conversely, pathways such as transcriptional regulation, fate commitment, and DNA methylation were significantly enriched in those Ribo-mRNAs that decreased over time. In addition, we validated the expression of mRNAs with high magnitude changes that may affect spine and axon development. Our approach is easily applicable to other conditions using overexpression or knockdown strategies.

## Material and Methods

### Animals

Research protocols were approved by the Yale University Institutional Animal Care and Use Committee. All experiments were performed on CD-1 (Charles River), an outbred strain of mice of either gender.

### *In utero* electroporation (somatosensory) and plasmids

Each DNA plasmid was diluted in sterile PBS (pH 7.4) to a final concentration of 1–2 μg/μl (specific concentrations below). About 1 μl of DNA solution, containing 0.1% fast green added as injection tracer, was injected into the lateral ventricle (LV) of E15.5 fetuses with a glass pipette. After injecting all fetuses in a single uterine horn with manual pressure, PBS soaked tweezer-type electrodes (model 520, BTX) were positioned on heads of the fetuses across the uterine wall and 5 square-pulses at 42 V, 50 ms duration, 950 ms intervals were applied using a pulse generator (ECM830, BTX). A DNA solution composed of pUB-BLRP-EGFP-L10a (2.0 μg/μl) and pCAG-tdTomato (1.0 μg/μl). Mice were prescreened for successful electroporation via expression of fluorescent protein on fluorescence enabled stereo microscope (SZX16, Olympus) prior to recruitment for immunostaining and TRAP.

### TRAP procedure

For each time point (P0, P7, and P14), TRAP samples were prepared in triplicates. Each sample was obtained from tdTomato-positive cortices microdissected from 6–8 pups. The protocols for the TRAP procedure have been described in detail in (Heiman et al., 2014). Modifications from the published protocol are presented below. The procedure was divided into the following sub-procedures.

**Brain lysate preparation (step 1, sub-steps iii-xi).—**iv: the tissue was homogenized with 30 full strokes. x: the post-mitochondrial supernatant (S20) was prepared by centrifugation at 4°C, 20 min, 16,000g.

**Immunoprecipitation (IP, steps 2–8):** GFP-Trap coupled to magnetic beads (super-high affinity Camelidae antibody fragments for GFP coupled to magnetic beads from Bulldog-Bio, GTN020) were used. Beads were washed three times in low-salt buffer prior to use. Step 3: we added 250 μl of freshly resuspended beads to each S20 sample (~1 ml). Step 4: the solution was then incubated at 4°C overnight with gentle mixing in a tube rotator. Step 5–7: as published (several rounds of beads collection with magnet and washes); Step 8: The beads were resuspended in 100 μl Nanoprep Lysis Buffer with 0.7 μ β-ME (use lysis buffer from the Stratagene Absolutely RNA Nanoprep kit), vortex, incubate for 10 min at room temperature, remove the RNA (in the lysis buffer) from the beads with the magnet and proceed to RNA cleanup.

**RNA clean-up and quantification (step 9–11):** Following a 10 min-incubation, the beads were collected with a magnet, and the supernatant transferred to a new microcentrifuge tube at room temperature. An equal volume of 80% sulfolane was added to the supernatant and vortexed (5 s). The mixture was transferred to a seated RNA-binding

nano-spin cup and microcentrifuged at 16,000g for 60 s. After retaining the spin cup and discarding the filtrate, 300 μl of 1x Low-Salt Wash Buffer was added and then the solution was spun in a microcentrifuge at 16,000g for 60 s. The procedure was repeated and the solution spun for 2 min to dry the filter. Then it was gently mixed with 2.5 μl of reconstituted RNase-Free DNase I and 12.5 μl of DNase Digestion Buffer. The 15 μl of DNase solution was directly added onto the fiber matrix of the spin cup and then incubated at 37°C for 15 min. The low salt wash buffer procedure was then repeated three times. After the wash and a 3 min spin to dry to the fiber matrix, the spin cup was transferred to a fresh 2-ml collection tube, into which a 20 μl of Elution Buffer heated to 60°C was added and incubated for 2 min at room temperature. It was then spun in a microcentrifuge at 16,000g for 5 min. The purified RNA in the eluate in the collection tube was transferred to a capped microcentrifuge tube. 2 μl aliquots were used for the first round of QC using a spectrophotometer (Nanodrop, ND-1000, ThermoScientific). The rest of the sample was stored at −80°C.

**Sub-procedure for plasmid and IP validation using GFP-trap magnetic beads:** After preparing the brain lysate, a small aliquot of S20 (50–100 μl) was saved to be used as the unbound fraction (or input) for western blot. After step 7 of the IP sub-procedure (collection of beads using a magnet and multiple washes), the beads were resuspended in 50 μl 2x SDS-sample buffer, boiled for 10 min at 95°C to dissociate the immunocomplexes from the beads. The beads were then magnetically separated and SDS-PAGE was performed with the supernatant referred to as bound fraction for western blot.

## Microarray and analysis

We ran RNA samples using an Agilent RNA 6000 Pico Kit on an Agilent 2100 Bioanalyzer to check for quality. Preparation of labeled cRNA for hybridization onto Mouse Gene 2.0 ST and WT PLUS Kit (#902463, Affymetrix) was as recommended (Affymetrix protocol) using the GeneChip™ WT cDNA synthesis and amplification kit (Affymetrix). The array hybridization was performed by the Yale Center for Genome Analysis. Microarray data were processed using the Bioconductor/R package oligo (Carvalho and Irizarry, 2010). Raw intensities were normalized using transposed robust multichip average (tRMA)(Giorgi et al., 2010). For further analysis, only main probes with signals above background in at least 3 samples were used. Threshold for background was determined using the median intensity of the anti-genomic probesets. Oligodendrocyte and astrocyte- specific genes above background (20-fold enrichment from (Cahoy et al., 2008)) (39 and 60, respectively) were also filtered out. Differentially expressed genes were determined using the Bioconductor/R package limma (Ritchie et al., 2015). Genes with Benjamini-Hochberg (BH) corrected $P<0.05$ and a log fold change of greater than 0.5 or less than - 0.5 log fold change ($\pm$ 1.41 natural fold change) were considered differentially expressed. All heatmaps were generated with the gplots package with Rcolorbrewer in R. Genes were clustered using Pearson correlation and complete linkage. Gene ontology enrichment analysis was performed using the topGO Bioconductor/R package(Alexa et al., 2006) using the "weight01" algorithm with Fisher exact test. GO terms with a BH corrected $P < 0.05$ were considered significantly enriched. The gene universe included all genes represented on the chipset with signals above background. Fold enrichment was determined by dividing the number of differentially

expressed genes from our gene list that belong to a GO term divided by the expected number of genes from that GO term.

## Brain slice preparation and immunostaining

Mice were given a lethal injection of pentobarbital (150 mg/kg) and perfused transcardially with ice cold phosphate buffered saline (PBS, pH 7.4) followed by ice cold paraformaldehyde (PFA, 4%). Perfused brains were dissected and dropped fixed in 4% PFA for overnight. Then, fixed brains were transferred to a solution of 30% sucrose in PBS. Following equilibration of the tissue in the sucrose solution, brains were sectioned coronally on a freezing sliding microtome at a thickness of 50 μm. Sections were stored in cryoprotectant at −20°C.

For immunofluorescence, free-floating sections were blocked for 1 hour at room temperature in blocking buffer consisting of 2% bovine serum albumin and 0.1% Triton X in PBS and then incubate with primary antibodies (rabbit anti-ER81, Covance PRB-362C, 1:10000) diluted in blocking buffer overnight at 4°C. Sections were washed with PBS containing 0.05% Tween 20 and then placed in blocking buffer containing secondary antibodies (Alexa Fluor conjugated 647, 1:1000) for 1 hour at room temperature. DAPI was added to the secondary antibody incubation at 1:5000. ProLong Gold (Invitrogen) was used to mount and preserve stained sections. Stained sections were imaged using a fluorescence confocal microscope (FV1000, Olympus). Z-stack images were acquired on the confocal microscope with 10x and 20x dry objective (Olympus). Images were reconstructed using ImageJ and Photoshop.

## Western blots from fresh cortices

Whole cortical hemispheres were collected from three different litters from three different dams at postnatal day (P) 0, P7, and P14, with 2–4 mice representing each age group per litter. Mie were deeply anesthetized with isoflurane and whole cortical hemispheres were rapidly dissected in ice-cold phosphate buffered saline (PBS;137 mM NaCl, 2.7 mM KCl, 4.3 mM Na2HPO4, 1.47 mM KH2PO4, pH 7.4) and flash frozen in dry ice. All samples were stored at −80°C until used. Whole cortices from one hemisphere were homogenized in ice-cold homogenization buffer (100 mM Tris-HCl, pH 7.4, 0.32 M sucrose, 1 mM EDTA, 5 mM HEPES) containing protease and phosphatase inhibitor cocktail tablets (Roche). Total protein concentration of the samples was determined using the Pierce BCA protein assay kit (ThermoFisher). Samples were prepared for SDS-PAGE by dilution in Laemmli buffer (4X: 0.25M Tris-HCl, pH 6.8, 6% SDS, 40% sucrose, 0.04% bromophenol blue, 200 mM dithiothreitol) and 100 mM Tris-HCl, pH 7.4. Equal amount of proteins (10 μg) per sample were resolved by SDS-PAGE on 4–15% gradient gels (Bio-Rad) and transferred onto PVDF membranes (Bio-Rad). Total protein staining were performed using SYPRO ruby fluorescent stain (Bio-Rad) and captured on a Kodak Image Station 4000 MM PRO. Membranes were then incubated in blocking buffer (5% non-fat milk, 1mM Na3VO4 in PBS+0.1% Tween 20) for 1 hour at room temperature, in primary antibodies overnight at 4°C, and in secondary antibodies for 1 hour at room temperature. Membranes were washed 3×10 min in PBS+0.1% Tween 20 between each step. Immunoreactive bands were developed using enhanced chemiluminescence reagents (Thermo Scientific) and captured on blue autoradiography

films (WorldWide Medical Products). Relative quantification was performed using Image J software (NIH). Total proteins stains were quantified by measuring an equal sized strip through the center of each lane running from top to bottom of the blot. Background values taken between the lanes were subtracted from the total protein measurements. For each antibody, optical densities of immunoreactive bands were quantified by measuring equal sized boxed drawn around each band. Background values taken beneath the bands were subtracted from these measurements. Each immunoreactive band was normalized to the total protein levels within the same lane for loading control. Results were expressed as percentages of P14 mice (% control).

### Antibodies

Antibodies are listed in **Table 1**.

### Statistical analyses

Microarray data analysis is detailed above. One-way ANOVA with Tukey's post hoc test was performed using Prism 7 software (GraphPad) for the western blot data. The significance level was set at $p < 0.05$. Data are presented as mean ± standard error of the mean (SEM).

## Results

### IUE-based TRAP (iTRAP) from layer 2–4 cortical pyramidal neurons

To perform TRAP analysis of layer-specific cortical neurons at different postnatal ages, we performed IUE of a plasmid encoding enhanced (E) GFP-tagged ribosomal protein L10a using the human Ubiquitin C (UbiC) promoter. IUE of pUbiC-EGFP-L10a was performed at E14-E15 to preferentially target layer 2–4 cortical pyramidal neurons as illustrated in a coronal section from a P14 mouse (E15 IUE in Fig. 1A). A higher magnification photograph of EGFP fluorescence revealed puncta within the nucleoli, the sites of ribosomal biogenesis (Fig. 1B). To confirm functional integration of EGFP-L10a, we microdissected EGFP-fluorescent cortices at different postnatal ages and performed anti-EGFP immunoprecipitations (IPs) to purify mRNA bound to ribosomes (Ribo-mRNA). For each time point (P0, P7, and P14), 6–8 microdissected, fluorescent cortices were pooled into one sample for IP. Then, IPs were performed on three samples for each time point. We also performed IUE of regular EGFP plasmid as control. On immunoblots, the IP-derived fraction displayed enrichment in EGFP-L10a or EGFP in the respective conditions (Fig. 1C). In addition, IPs from EGFP-L10a-expressing cortices resulted in significant RNA yields (a range of 32 to 178 ng total RNA per EGFP-L10a IP quantified using a Nanodrop; data not shown), suggesting that EGFP-L10a was incorporated into ribosomes of the electroporated neurons. IP from EGFP-expressing cortices also yield a small amount of RNA (<10% of the RNA quantity using EGFP-L10a), in particular at P14 (see discussion), suggesting that the EGFP-L10a IP may be contaminated with unbound mRNA. RNA was of high quality based on the 28S/18S ratio (above 2 for all samples) and the RNA integrity number (range 9.7–10) calculated using the 2100 Bioanalyzer (Fig. 1D). Finally, we performed RT-PCR to examine whether our Ribo-mRNA was indeed enriched in upper layer neuron marker compared to total RNA obtained from non-electroporated cortices. *Cux1*, a marker of layer 2–4 neurons (Nieto et al., 2004) was enriched compared to a maker of deep layer neurons, *Bcl11b* (Fig.

1E). In addition, the endothelial gene, *Notch4*, was not detected in Ribo-RNA while it was present in total RNA. Collectively these data validated the quality of Ribo-mRNA and the enrichment in upper layer neuron genes. Ribo-mRNA from each IP was then processed for gene profiling.

### Microarray and gene ontology analyses

The principal component analysis (PCA) of microarray data showed that samples from the same age group clustered together (Fig. 2A). We provide the array containing all the genes above background levels (26,203 genes). Gene profiling identified 7,326 genes in the targeted neurons that were significantly altered during neonatal development. We found that 2981, 3440, and 6550 neuronal genes were altered from P0 to P7 (notated as P0–P7), P7–14, and P0–P14, respectively (Supplemental Tables 2-4, astrocytes and oligodendrocytes gene were filtered out). iTRAP is expected to provide an enrichment for the genes in pyramidal neurons, which contain EGFP-L10a. Nevertheless, contamination occurs and as such we also provide a list of genes above background from cell types other than pyramidal neurons, including astrocytes (61 genes), oligodendrocytes (39 genes) (based on (Cahoy et al.), GABAergic interneurons (7 classic interneuron markers), microglia (242) and endothelial cells (190, based on (Zhang et al., 2014), Supplemental Table 5). 10–20% of the microglial genes detected changed with development. Around 3050% of the astrocyte and oligodendrocyte genes are differentially expressed in any given comparison, except the oligodendrocyte genes in the P7 vs. P0 comparison where only 10% of the oligo marker list is changed. For oligodendrocytes, essentially myelin genes are detected at P14 likely due to non-specific binding of myelin to the beads. Only 10–20% of the microglial genes and 8–26% of the endothelial genes changed with development. Overall non-pyramidal genes were expressed in low numbers.

Many of the identified neuronal genes followed known developmental patterns based on literature search or the Allen Brain Atlas database. Genes selectively expressed in immature neurons like *Tbr1* (glutamatergic neurons), doublecortin (Dcx), *CD24a*, neuron-specific class III β-tubulin *(Tubb3* or Tuj1), and *Ncam1* significantly decreased with development while markers of mature neurons, *Rbfox3* (NeuN), *Eno2* (NSE), and *Camk2a* significantly increased (Fig. 2B). In addition, the expression of many neuronal ion channels important for the generation of action potentials (voltage-gated K$^+$, Na$^+$ [e.g., *Scn1b]* and Ca$^{2+}$ [e.g., *Cacng3]* channels) and synaptic proteins (e.g., PSD95 *[Dlg4]*, Synapsin 1 *[Syn1]*, VGlut1 [Scl17a7]) significantly increased during development with large increases from P0 to P7 (see array data in Supplemental data). To validate some of the array results, we used western blots from cortical lysates to examine two well-characterized synaptic proteins, Dlg4 (PSD-95) and synapsin-1. First, we examined whether some classical loading controls, GAPDH, β-tubulin, and vinculin, for whole cell lysate could be used. All three commonly used loading controls significantly changed over time on immunoblots (data not shown) despite not significantly increasing in the array. This is likely due to the increase in cell number and size during corticogenesis. We thus decided to use a total protein stain as loading controls. We then found that Dlg4 and synapsin-1, significantly increased with development (Fig. 2B). The most significant increase was from P0 to P7 when neurons are getting primed for developing spines and synapses.

We next performed gene ontology analysis to compare to expected development milestones. Figure 3 outlines the top 10 lists for biological processes (BP) and cellular components (CC) annotations amongst upregulated and downregulated genes at P0–P7 and P7–P14. These lists contain the 10 GO terms that have the lowest p-values when testing for significantly enriched terms. Both time point comparisons shared several CC terms amongst up- and downregulated transcripts. Analysis of upregulated mRNAs showed overrepresentation of CC terms including cell junction (e.g., anchoring proteins and receptors such as neurotransmitters), voltage-gated $K^+$ channel complex, postsynaptic membrane and neuronal postsynaptic density, dendrite and spine, presynaptic active zone (P0–P7) and paranode region (P7–P14). Enriched CC terms among downregulated transcripts are largely related to the nucleus, chromatin, and chromosome. In transcripts upregulated over time, overrepresented BP terms include regulation of ion transmembrane transport, synaptic transmission and regulation of synaptic plasticity, and nerve conduction primarily at P7–P14. BPs enriched among translating mRNAs that are decreasing over time include regulation of transcription, forebrain neuron fate commitment, DNA methylation, cell division, and axon guidance at P0–P7. These enriched terms correspond with expected changes seen during cortical pyramidal neuron development.

### Validation of mRNA identified to be age-dependent

We chose a set of gene products based on their significant fold change and their potential, previously unexplored function in neuronal development (see discussion). The selected targets are listed in Table 1 with their fold-change and illustrated in Figure 4. These include downregulated genes *St8sia2* and *Draxin*, biphasic regulated gene *Fkbp1b*, and upregulated genes *Lynx1, Nrn1* (Neuritin), *Cntnap1* (Caspr). We then compared these findings with those from western blots from whole cortex (N=8–9 samples per time point, Figure 5). We found that only 2 (St8sia2 and FKBP1B) out of 6 gene products examined deviated slightly from the patterns obtained from the TRAP analysis. *St8sia2* decreased from both P0–P7 and P7–P14 in the array, but the gene product remained steady from P0–P7 using immunoblotting and FKBP1B remained stable from P7–P14 instead of decreasing in the array. Considering that 4 of the genes identified were recapitulated with immunoblotting, these data validate the TRAP-array results. The two genes that partly differed may emphasize the limitation of the immunoblotting using whole cortex as opposed to a cell type specific using TRAP as further discussed below.

## Discussion

Here, we combined TRAP with IUE (iTRAP) to access Ribo-mRNA in layer 2–4 pyramidal neurons as previously reported (Rannals et al., 2016). We provide the first comparison across neonatal development allowing us to identify novel genes and gene products that change as pyramidal neurons mature. Our approach was selective for layer 2–4 pyramidal neurons despite getting about 10% contamination with non-target RNA (i.e., RNA likely attached to the beads). This may be reduced using different GFP antibodies and beads. The GFP-based pull-down approach led to an enrichment in layer 2–4 marker and lack of endothelial marker by RT-PCR analysis, but a low level of contamination is anticipated. Indeed, we detected a few RNA from other cell types (glia, endothelial cells, and interneurons, less than 600 total

genes) that were expressed at low levels and are provided in the supplemental tables. The table includes the genes (10–50%) that changed during development. In addition, we detected significant changes in an abundant number of neuronal RNAs that increased or decreased as expected with neuron maturation. In particular, we found that Ribo-mRNA for synaptic proteins and ion channels as well as for morphogenic molecules significantly increased over time while markers of immature neurons decreased.

We also identified a series of molecules, the function of which remain understudied or unknown on neuronal development. Two of the molecules that decreased over time are ST8SIA2 and Draxin. ST8SIA2 is a neural cell adhesion molecule (NCAM)-specific polysialic acid (PSA) synthase. Loss of *St8sia2* significantly reduced polySia levels during the first postnatal days, when polySia expression reaches its peak in the wild-type brain (Galuska et al., 2006; Oltmann-Norden et al., 2008). *St8sia2* modifies the function of NCAM during neural development (Kojima et al., 1996a; Kojima et al., 1996b) and as such facilitates neurite outgrowth (Franceschini et al., 2001) and directs hippocampal axonal targeting important for fear behavior (Angata and Fukuda, 2003). Consistent with these data, loss of *St8sia2* caused several defects in brain connectivity (e.g., 50% reduction in the width of the anterior commissure) (Hildebrandt et al., 2009). Finally, variations in the *ST8SIA2* gene have been linked to schizophrenia (Arai et al., 2006; Tao et al., 2007). Draxin is a secreted protein acting as a repulsive guidance cue for axons in the forebrain and cerebellum (Islam et al., 2009). Draxin deficient mice have abnormal development of spinal cord and forebrain commissures as well as smaller hippocampus (Islam et al., 2009; Su et al., 2010). Draxin from neocortical neurons also controls the guidance of thalamocortical projections into the neocortex (Shinmyo et al., 2015). These published data match our finding of a progressive decline in *Draxin* expression over time. The fact that *Draxin* knockout mice have smaller hippocampi suggests additional, unexplored functions of Draxin.

*Fkbp1b* displayed a transient increase at P7 using the iTRAP approach. However, using western blot, FKBP1B increased from P0-P7 and then remained high. The discrepancy is unclear based on the unknown cellular expression of this protein. It is possible that increased expression of FKBP1B in glia during neonatal development would mask a neuron-specific decrease in western blots using lysates from the whole cortex. In terms of function, FKBP1B (also known as FK506-binding proteins 1b and FKBP12.6) is an immunophilin protein that binds ryanodine receptors and inhibits $Ca^{2+}$-induced $Ca^{2+}$ release and has been extensively studied for its physiological role in excitation-contraction coupling in cardiac muscle. It also binds the immunosuppressant drugs FK506 and rapamycin. It has been shown that declining FKBP function is a key factor in aging-related $Ca^{2+}$ dysregulation (Gant et al., 2018). However, a function on brain development remains to be examined. Considering its role in $Ca^{2+}$ homeostasis, it is plausible for FKBP1B to regulate neuronal migration and/or development of neuronal processes such as axons or dendrites.

We also explored three Ribo-mRNA encoding CNTNAP1, Lynx1, and NRN1 that increased as neurons matured. As with FKBP1B validation, small differences between the iTRAP and western blots can be easily explained by dilution in whole tissue lysates by astrocytes or other glial cells. CNTNAP1, also called contactin-associated protein CASPR, is a type I integral membrane protein that associates with contactin and is expressed exclusively by

neurons. Caspr is a major component of the septate junctions that form between axons and paranodal loops and is thus involved in the maintenance of the polarized domains of myelinated axons (Einheber et al., 1997). Lynx1 is a an endogenous prototoxin similar to α-bungarotoxin in snake venom and binds to the nicotinic acetylcholine receptor (nAChR) (Miwa et al., 1999). *Lynx1* has been reported to limit plasticity in adult visual cortex (Morishita et al., 2010) and limit spine turnover in adult animals (Sajo et al., 2016). A function of Lynx1 in younger animals remains unclear. NRN1, neuritin 1 also known as candidate plasticity gene 15 (CPG15), is an activity- dependent small extracellular protein that is anchored to the cell surface by a glycosyl- phosphoinositide link (Naeve et al., 1997). Several studies showed its role in neurite extension, axon branching and more recently neuronal migration (see (Shimada et al., 2016) for references). In addition, NRN1 variability is a shared risk factor for both schizophrenia-spectrum disorders (SSD) and bipolar disorders and NRN1 may have a selective impact on age at onset and intelligence in SSD (Fatjo-Vilas et al., 2016).

## Conclusions

Collectively, our findings highlight iTRAP tool as a way to identify actively translated genes across neuron development in a temporally and cell-type specific manner. Further, this approach can reveal genes that were previously not known to have a role in neuronal maturation. The approach can be combined with specific knockout or overexpression vectors to track pathway changes that affect selective developmental processes (e.g., calcium homeostasis) important for brain development and with cell type-specific or activity-dependent promoters to drive the expression of EGFP-L10a in specific subsets of pyramidal neurons or in an activity-dependent manner. Finally, the approach is a powerful way to track and identify cell and stage specific changes in gene expression that precede or promote pathogenesis in animal models of neurodevelopmental disorders.

## Supplementary Material

Refer to Web version on PubMed Central for supplementary material.

## Acknowledgments

## Glossary

| | |
|---|---|
| **IUE:** | in utero electroporation |
| **TRAP:** | translating ribosome affinity purification |
| **P:** | postnatal |
| **E:** | embryonic |
| **PCA:** | principal component analysis |

**Ribo-mRNA:**  ribosome bound mRNA

## References

Alexa A, Rahnenfuhrer J, Lengauer T, 2006 Improved scoring of functional groups from gene expression data by decorrelating GO graph structure. Bioinformatics 22, 1600–1607. [PubMed: 16606683]

Angata K, Fukuda M, 2003 Polysialyltransferases: major players in polysialic acid synthesis on the neural cell adhesion molecule. Biochimie 85, 195–206. [PubMed: 12765789]

Arai M, Yamada K, Toyota T, Obata N, Haga S, Yoshida Y, Nakamura K, Minabe Y, Ujike H, Sora I, Ikeda K, Mori N, Yoshikawa T, Itokawa M, 2006 Association between polymorphisms in the promoter region of the sialyltransferase 8B (SIAT8B) gene and schizophrenia. Biol Psychiatry 59, 652–659. [PubMed: 16229822]

Cahoy JD, Emery B, Kaushal A, Foo LC, Zamanian JL, Christopher son KS, Xing Y, Lubischer JL, Krieg PA, Krupenko SA, Thompson WJ, Barres BA, 2008 A transcriptome database for astrocytes, neurons, and oligodendrocytes: a new resource for understanding brain development and function. J Neurosci 28, 264–278. [PubMed: 18171944]

Carvalho BS, Irizarry RA, 2010 A framework for oligonucleotide microarray preprocessing. Bioinformatics 26, 2363–2367. [PubMed: 20688976]

Cook-Snyder DR, Jones A, Reijmers LG, 2015 A retrograde adeno-associated virus for collecting ribosome-bound mRNA from anatomically defined projection neurons. Front Mol Neurosci 8, 56. [PubMed: 26557053]

Drane L, Ainsley JA, Mayford MR, Reijmers LG, 2014 A transgenic mouse line for collecting ribosome-bound mRNA using the tetracycline transactivator system. Front Mol Neurosci 7, 82. [PubMed: 25400545]

Einheber S, Zanazzi G, Ching W, Scherer S, Milner TA, Peles E, Salzer JL, 1997 The axonal membrane protein Caspr, a homologue of neurexin IV, is a component of the septate-like paranodal junctions that assemble during myelination. Journal of cell Biology 139, 1495–1506. [PubMed: 9396755]

Fatjo-Vilas M, Prats C, Pomarol-Clotet E, Lazaro L, Moreno C, Gonzalez-Ortega I, Lera-Miguel S, Miret S, Munoz MJ, Ibanez I, Campanera S, Giralt-Lopez M, Cuesta MJ, Peralta V, Ortet G, Parellada M, Gonzalez-Pinto A, McKenna PJ, Fananas L, 2016 Involvement of NRN1 gene in schizophrenia-spectrum and bipolar disorders and its impact on age at onset and cognitive functioning. World J Biol Psychiatry 17, 129–139. [PubMed: 26700405]

Franceschini I, Angata K, Ong E, Hong A, Doherty P, Fukuda M, 2001 Polysialyltransferase ST8Sia II (STX) polysialylates all of the major isoforms of NCAM and facilitates neurite outgrowth. Glycobiology 11, 231–239. [PubMed: 11320061]

Galuska SP, Oltmann-Norden I, Geyer H, Weinhold B, Kuchelmeister K, Hildebrandt H, Gerardy-Schahn R, Geyer R, Muhlenhoff M, 2006 Polysialic acid profiles of mice expressing variant allelic combinations of the polysialyltransferases ST8SiaII and ST8SiaIV. J Biol Chem 281, 31605–31615. [PubMed: 16940046]

Gant JC, Blalock EM, Chen KC, Kadish I, Thibault O, Porter NM, Landfield PW, 2018 FK506-Binding Protein 12.6/1b, a Negative Regulator of [Ca(2+)], Rescues Memory and Restores Genomic Regulation in the Hippocampus of Aging Rats. J Neurosci 38, 1030–1041. [PubMed: 29255009]

Giorgi FM, Bolger AM, Lohse M, Usadel B, 2010 Algorithm-driven artifacts in median polish summarization of microarray data. BMC. Bioinformatics 11, 553. [PubMed: 21070630]

Heiman M, Kulicke R, Fenster RJ, Greengard P, Heintz N, 2014 Cell type-specific mRNA purification by translating ribosome affinity purification (TRAP). Nat. Protoc 9, 1282–1291. [PubMed: 24810037]

Heiman M, Schaefer A, Gong S, Peterson JD, Day M, Ramsey KE, Suarez-Farinas M, Schwarz C, Stephan DA, Surmeier DJ, Greengard P, Heintz N, 2008 A translational profiling approach for the molecular characterization of CNS cell types. Cell 135, 738–748. [PubMed: 19013281]

Hildebrandt H, Muhlenhoff M, Oltmann-Norden I, Rockle I, Burkhardt H, Weinhold B, Gerardy-Schahn R, 2009 Imbalance of neural cell adhesion molecule and polysialyltransferase alleles causes defective brain connectivity. Brain 132, 2831–2838. [PubMed: 19443631]

Islam SM, Shinmyo Y, Okafuji T, Su Y, Naser IB, Ahmed G, Zhang S, Chen S, Ohta K, Kiyonari H, Abe T, Tanaka S, Nishinakamura R, Terashima T, Kitamura T, Tanaka H, 2009 Draxin, a repulsive guidance protein for spinal cord and forebrain commissures. Science 323, 388–393. [PubMed: 19150847]

Kojima N, Kono M, Yoshida Y, Tachida Y, Nakafuku M, Tsuji S, 1996a Biosynthesis and expression of polysialic acid on the neural cell adhesion molecule is predominantly directed by ST8Sia II/STX during in vitro neuronal differentiation. J Biol Chem 271, 22058–22062. [PubMed: 8703013]

Kojima N, Tachida Y, Yoshida Y, Tsuji S, 1996b Characterization of mouse ST8Sia II (STX) as a neural cell adhesion molecule-specific polysialic acid synthase. Requirement of core alpha1,6-linked fucose and a polypeptide chain for polysialylation. J Biol Chem 271, 19457–19463. [PubMed: 8702635]

Kwan KY, Sestan N, Anton ES, 2012 Transcriptional co-regulation of neuronal migration and laminar identity in the neocortex. Development 139, 1535–1546. [PubMed: 22492350]

Miwa JM, Ibanez-Tallon I, Crabtree GW, Sanchez R, Sali A, Role LW, Heintz N, 1999 lynx1, an endogenous toxin-like modulator of nicotinic acetylcholine receptors in the mammalian CNS. Neuron 23, 105–114. [PubMed: 10402197]

Molyneaux BJ, Arlotta P, Menezes JR, Macklis JD, 2007 Neuronal subtype specification in the cerebral cortex. Nat. Rev. Neurosci 8, 427–437. [PubMed: 17514196]

Morishita H, Miwa JM, Heintz N, Hensch TK, 2010 Lynx1, a cholinergic brake, limits plasticity in adult visual cortex. Science 330, 1238–1240. [PubMed: 21071629]

Naeve GS, Ramakrishnan M, Kramer R, Hevroni D, Citri Y, Theill LE, 1997 Neuritin: a gene induced by neural activity and neurotrophins that promotes neuritogenesis. Proc Natl Acad Sci U S A 94, 2648–2653. [PubMed: 9122250]

Nieto M, Monuki ES, Tang H, Imitola J, Haubst N, Khoury SJ, Cunningham J, Gotz M, Walsh CA, 2004 Expression of Cux-1 and Cux-2 in the subventricular zone and upper layers II-IV of the cerebral cortex. J Comp Neurol 479, 168–180. [PubMed: 15452856]

Oltmann-Norden I, Galuska SP, Hildebrandt H, Geyer R, Gerardy-Schahn R, Geyer H, Muhlenhoff M, 2008 Impact of the polysialyltransferases ST8SiaII and ST8SiaIV on polysialic acid synthesis during postnatal mouse brain development. J Biol Chem 283, 1463–1471. [PubMed: 18045870]

Rannals MD, Page SC, Campbell MN, Gallo RA, Mayfield B, Maher BJ, 2016 Neurodevelopmental models of transcription factor 4 deficiency converge on a common ion channel as a potential therapeutic target for Pitt Hopkins syndrome. Rare Dis 4, e1220468. [PubMed: 28032012]

Ritchie ME, Phipson B, Wu D, Hu Y, Law CW, Shi W, Smyth GK, 2015 limma powers differential expression analyses for RNA-sequencing and microarray studies. Nucleic Acids Res 43, e47. [PubMed: 25605792]

Sajo M, Ellis-Davies G, Morishita H, 2016 Lynx1 Limits Dendritic Spine Turnover in the Adult Visual Cortex. J Neurosci 36, 9472–9478. [PubMed: 27605620]

Shimada T, Yoshida T, Yamagata K, 2016 Neuritin Mediates Activity-Dependent Axonal Branch Formation in Part via FGF Signaling. J Neurosci 36, 4534–4548. [PubMed: 27098696]

Shinmyo Y, Asrafuzzaman Riyadh M, Ahmed G, Bin Naser I, Hossain M, Takebayashi H, Kawasaki H, Ohta K, Tanaka H, 2015 Draxin from neocortical neurons controls the guidance of thalamocortical projections into the neocortex. Nat Commun 6, 10232. [PubMed: 26659141]

Su Y, Zhang S, Islam SM, Shinmyo Y, Naser IB, Ahmed G, Tanaka H, 2010 Draxin is involved in the proper development of the dI3 interneuron in chick spinal cord. Dev Dyn 239, 1654–1663. [PubMed: 20503362]

Tabata H, Nakajima K, 2001 Efficient in utero gene transfer system to the developing mouse brain using electroporation: visualization of neuronal migration in the developing cortex. Neuroscience 103, 865–872. [PubMed: 11301197]

Tao R, Li C, Zheng Y, Qin W, Zhang J, Li X, Xu Y, Shi YY, Feng G, He L, 2007 Positive association between SIAT8B and schizophrenia in the Chinese Han population. Schizophr Res 90, 108–114. [PubMed: 17126533]

Zhang Y, Chen K, Sloan SA, Bennett ML, Scholze AR, O'Keeffe S, Phatnani HP, Guarnieri P, Caneda C, Ruderisch N, Deng S, Liddelow SA, Zhang C, Daneman R, Maniatis T, Barres BA, Wu JQ, 2014 An RNA-sequencing transcriptome and splicing database of glia, neurons, and vascular cells of the cerebral cortex. J Neurosci 34, 11929–11947. [PubMed: 25186741]

## Highlights

- We combined TRAP with in utero electroporation

- We report developmental patterns of classical genes

- We identified developmental processes

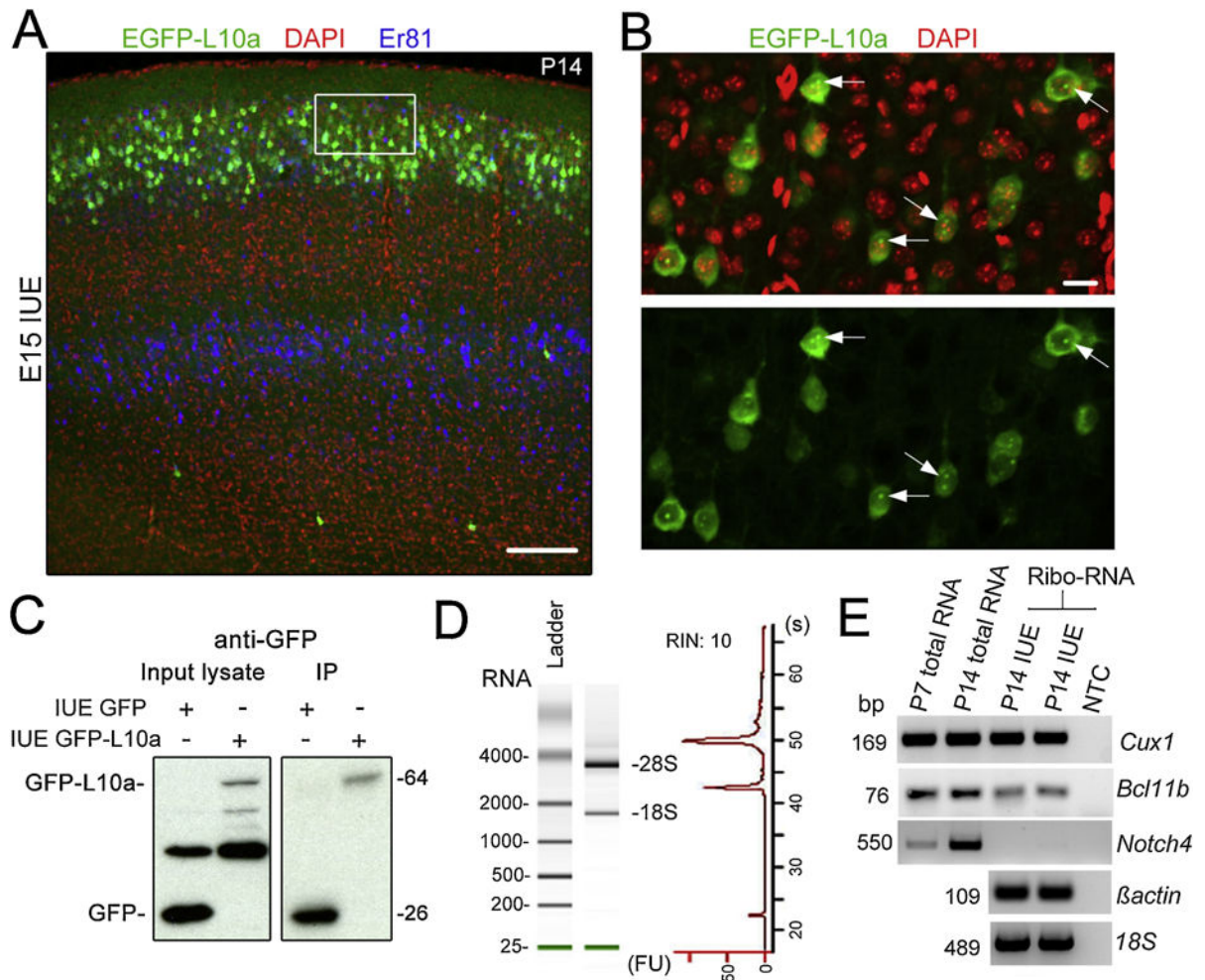- We identified specific developmental patterns for Ribo-mRNAs

**Figure 1.**

**(A)** Confocal images of EGFP-L10a fluorescence (green), DAPI (red) and Er81 (layer 5 marker, blue) immunostaining in a P14 coronal section. A plasmid encoding EGFAP-L10a was electroporated at E15. **(B)** Images of cortical neurons expressing EGFP-L10a and DAPI stain taken from the white square in (A). **(C)** Immunoblots for GFP from input lysate and lysate obtained after immunoprecipitation with GFP antibody. Lysates were from the cortex of mice electroporated with either GFP or GFP-L10a plasmid. **(D)** Representative RNA Bioanalyzer traces demonstrate the harvest of intact ribosomes, indicated by both large (28s) and small subunit (18s) ribosomal capture. **(E)** RT-PCR from total RNA obtained from cortex and Ribo-mRNA obtained after the TRAP procedure. P7 and 14 refers to the age at time of brain dissection from mice with or without IUE.
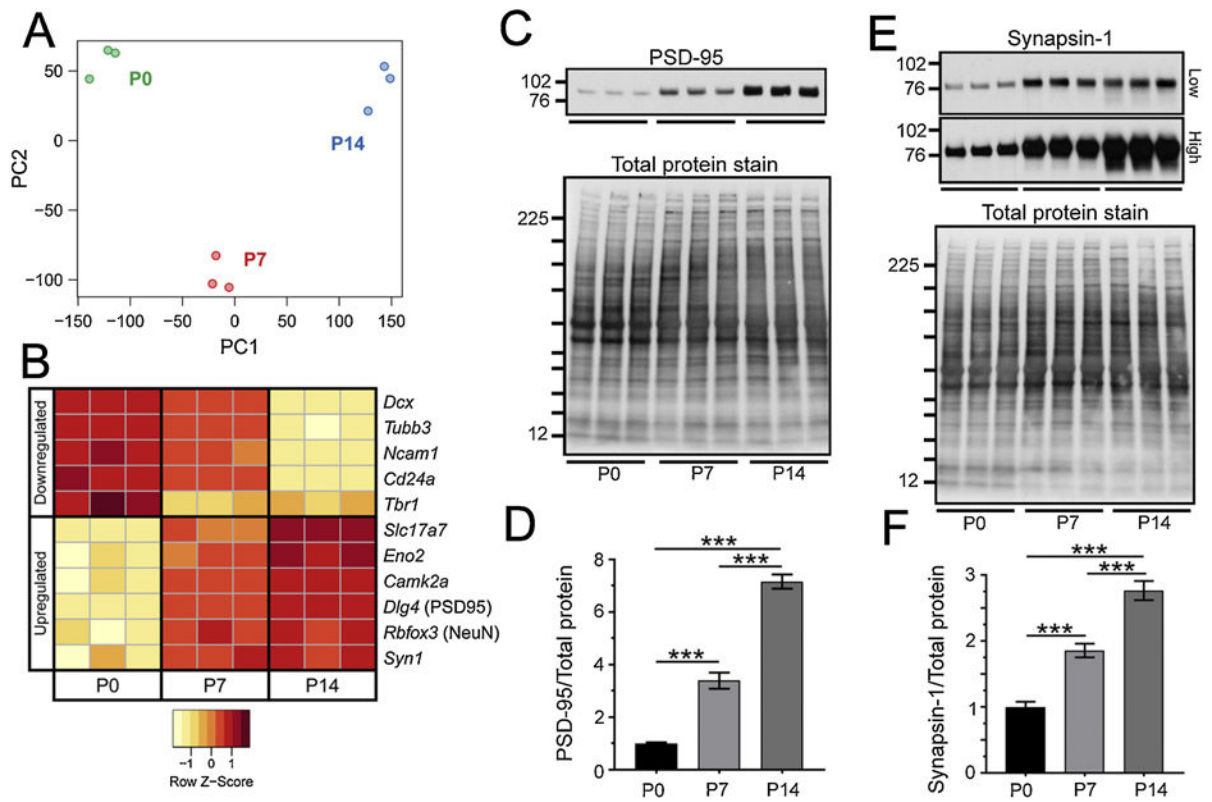
**Figure 2.**
**(A)** Principal component analysis (PCA) of microarray expression data. **(B)** Expression patterns of several neuronal RNA at P0, P7 and P14. **(C and E)** Western blots for PSD-95 and synapsin-1 over time and total protein stain used as a loading control. Low and high refer to the exposure time. **(D and F)** Quantification of the western blots in C and E, respectively.
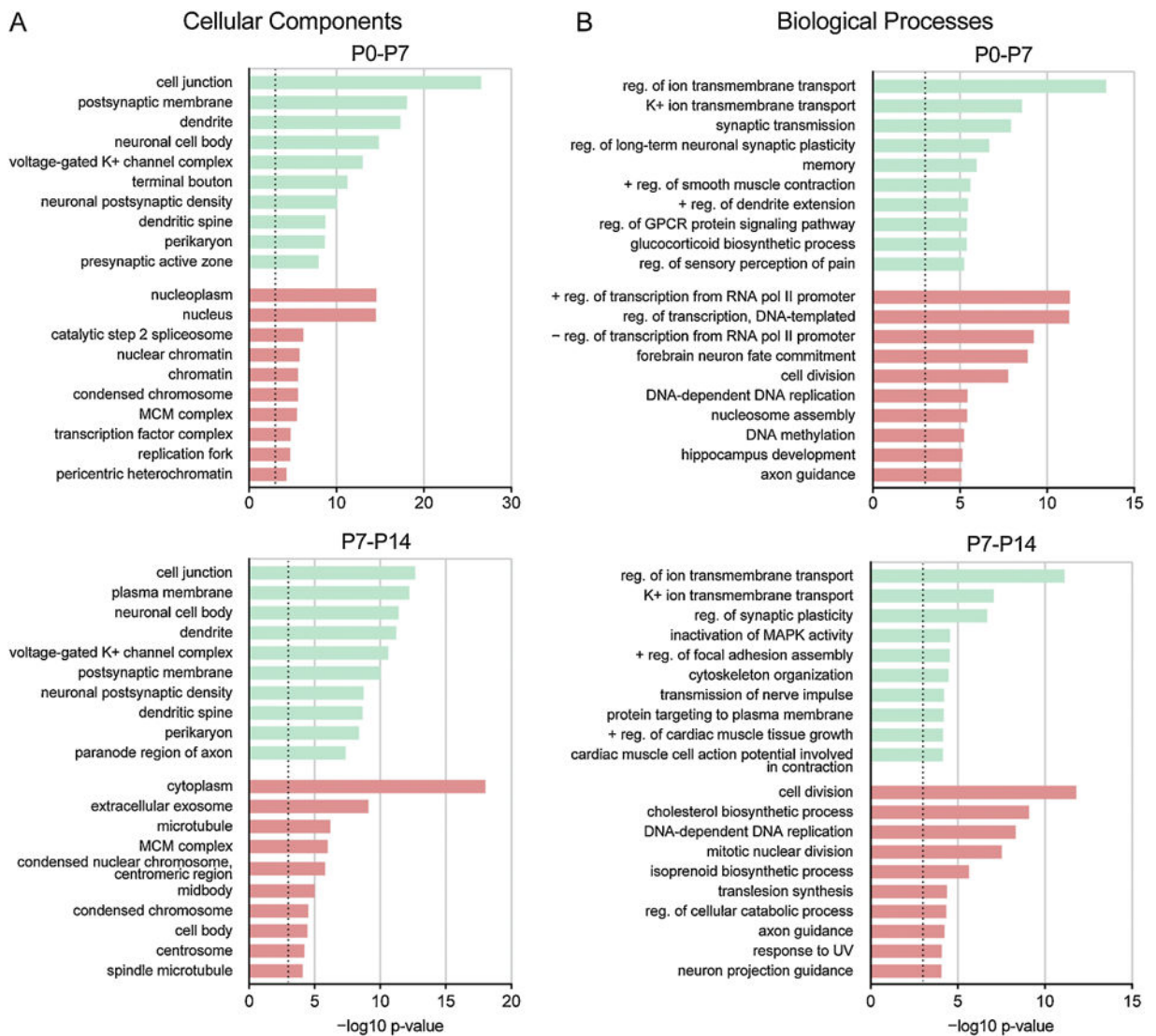
**Figure 3.**
Most significantly enriched GO terms for **(A)** cellular components and **(B)** biological processes in upregulated and downregulated Ribo-mRNA between P0-P7 and P7-P14. Green: terms enriched in upregulated transcripts. Red: terms enriched in downregulated transcripts. Dotted line represents $P<.001$.

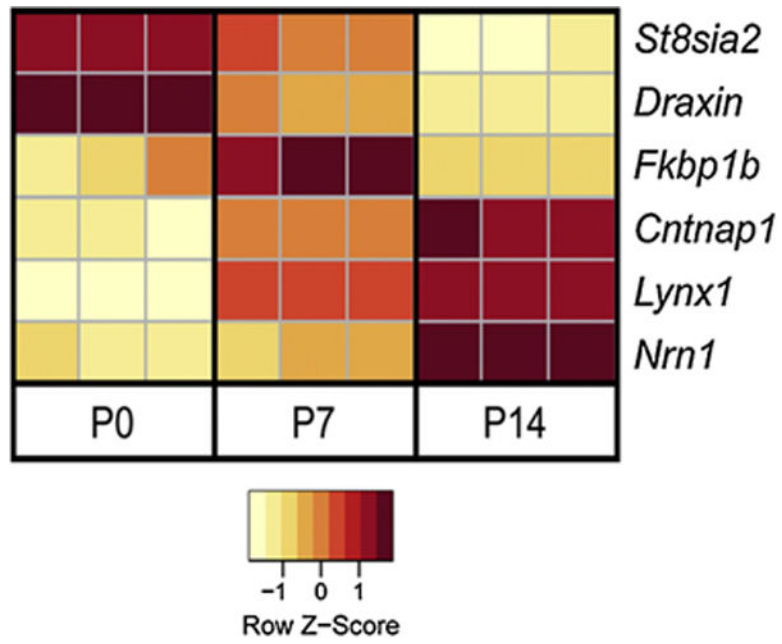**Figure 4.**
Expression patterns over time of Ribo-mRNAs that were not previously known to be developmentally regulated.
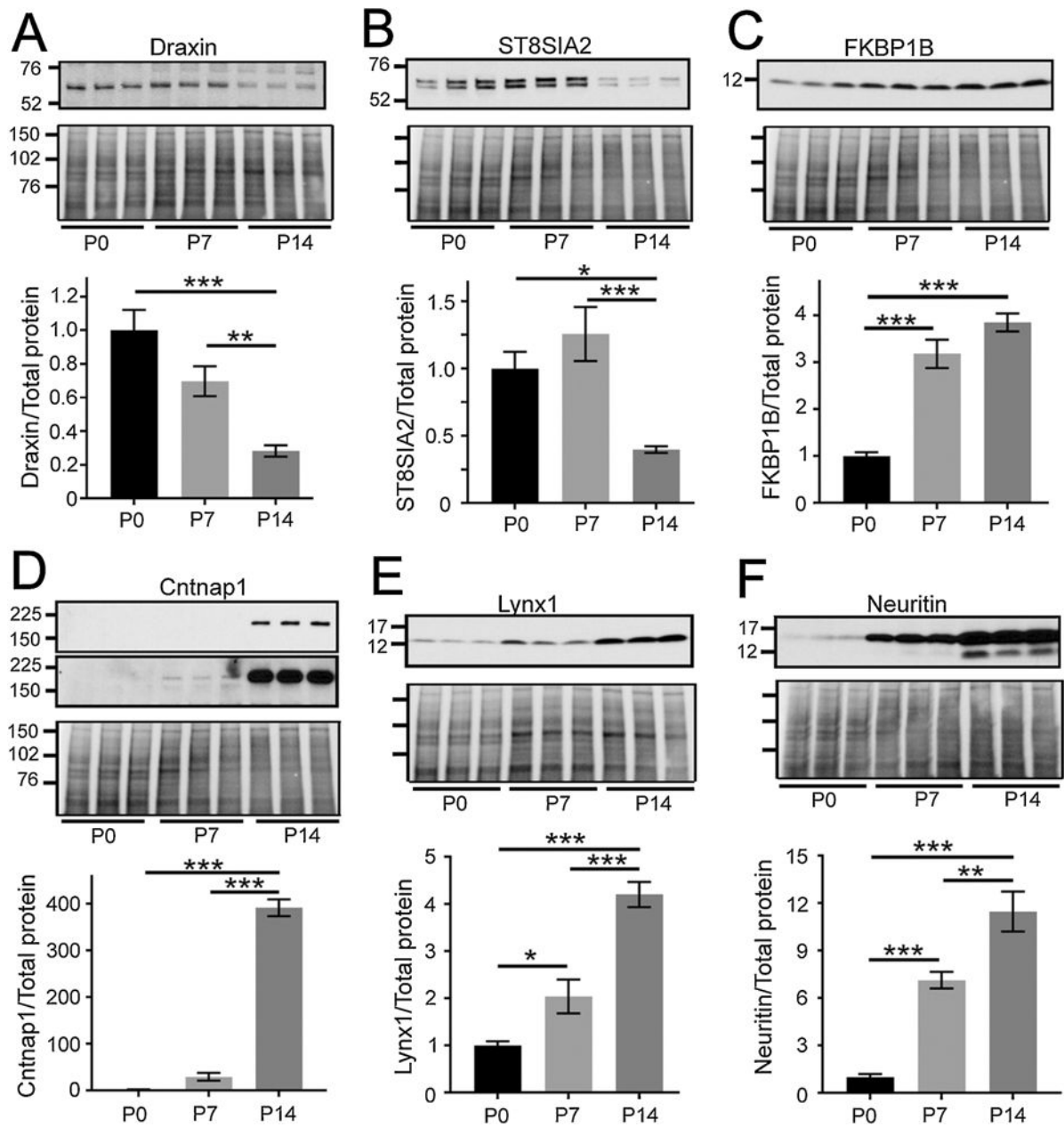
**Figure 5.**

Western blots for proteins of interest and cropped image of the total protein stain used as a loading control and quantifications of the ratio of each protein over the total protein normalized to the P0 time-point. Analysis was performed on the uncropped blot.

**Table 1.**

List of antibodies

| Primary Antibody | Company | Catalog Number | Dilution |
|---|---|---|---|
| Lynxl | Abcam | ab125035 | 1:1000 |
| Caspr (cntnapl) | Neuromab | 75–001 (K65/35) | 1:1000 |
| FKBP1B | Santa Cruz | sc-376135 | 1:100 |
| Neuritin | R&D systems | AF283 | 1:200 |
| Draxin | R&D systems | AF6148 | 1:200 |
| hST8SIA2 | R&D systems | AF6590 | 1:500 |
| PSD-95 | Cell Signaling | 3450 | 1:2000 |
| Synaptin-1 | Cell Signaling | 5297 | 1:2000 |
| β-tubulin | Cell signaling | 2128 | 1:2000 |
| GAPDH | Cell Signaling | 5174 | 1:5000 |
| GFP | Abcam | ab290 | 1:1000 |
| Vinculin | Cell signaling | 13901 | 1:5000 |

**Table 2.**

Fold change (FC) for genes shown in Figure 4 and 5.

| Gene symbol | FC P0–P7 | FC P7–P14 | FC P0–P14 |
|---|---|---|---|
| *Lynx1* | *+ 10.6* | *+2.0* | *+20.9* |
| *Nrn1* | *+ 1.5* | *+11.2* | *+17.5* |
| *Cntnap1* | *+5.9* | *+6.1* | *+36.4* |
| *St8sia2* | *−4.3* | *− 7.7* | *− 33* |
| *Draxin* | *− 6* | *−2.8* | *− 17.4* |
| *Fkbp1b* | *+2.7* | *−2.8* | *n.s.* |